Hofmeister effect and the phase diagram of lysozyme

S. Lettieri, Xiaofei Li, and J. D. Gunton
Department of Physics, Lehigh University, Bethlehem, Pennsylvania 18015, USA
(Received 5 March 2008; published 29 July 2008)

The phase diagrams for lysozyme are calculated for two different precipitant salts, NaCl and NaSCN, using a potential of mean force that takes into account contributions from ion-dispersion forces [M. Boström *et al.*, J. Phys. Chem. B **110**, 24757 (2006)]. Our results are consistent with a recent perturbation theory calculation (referenced above) in that the phase diagram for lysozyme with NaCl is quite different than for lysozyme with NaSCN for the same molar concentration (0.2 M). However, in contrast to the perturbation theory calculation, we find that the lysozyme phase diagram with NaCl has a metastable fluid-fluid coexistence curve and that the metastability gap in the case of NaSCN is much larger than predicted by perturbation theory.

DOI: 10.1103/PhysRevE.78.011921 PACS number(s): 87.15.ak, 87.15.km, 87.15.kr, 87.15.Zg

I. INTRODUCTION

In the late 1800s, Hofmeister and his colleagues [1] found that salts with common cation (positive ion) but different anions (negative ions) have different levels of effectiveness in stabilizing colloidal solutions. These salt anions can be arranged in a universal sequence known as the Hofmeister series. This effect is of widespread importance, including the precipitation of proteins from solution, the surface tension of salt solutions, ions binding to micelles, colloid stability, transport across red blood cells, and the cutting efficiency of DNA in buffered salt solutions (see, e.g., [2,3] for references). Understanding the Hofmeister effect has been a major challenge for theorists, since the classical Derjaguin-Landau-Verwey-Overbeek (DLVO) theory of interparticle interactions in colloid science depends only on the salt concentration and not on the salt type. This theory treats colloid stability in terms of a balance between attractive van der Waals forces and repulsive double-layer forces between the solute particles. Many phenomenological arguments have been proposed to explain the Hofmeister effects, including the idea that ions exert their effect indirectly by changing the water structure. For example, one talks about "chaotropic" and "cosmotropic" ions, "hard and soft ions," etc. None of these ideas, however, has produced a quantitative theory of the effect. However, in 1997, Ninham and Yaminsky [4] proposed that the ionic dispersion potential between the salt ion and solute particle, neglected in the DLVO theory, might provide a partial explanation of the Hofmeister effect. Since then, a series of papers have been written applying this idea to a variety of examples of the Hofmeister effect, including the important case of globular proteins in solution [2,3,5–9].

Understanding the Hofmeister effect in globular proteins in aqueous electrolyte solutions is of particular importance, since the phase transitions, self-assembly, and aggregation of proteins in solution are of fundamental and practical importance [2]. For example, it is important to understand the initial conditions necessary to grow high-quality protein crystals, including the important role of the precipitating agent, such as salt, in order to prepare defect-free samples that are suitable for x-ray crystallography. In addition, there are several diseases that result from undesired protein condensation (aggregation) from solution. These include sickle cell anemia [10–12], certain types of cataracts [13,14], and Alzheimer's disease [15,16]. Thus, understanding the physical conditions that led to such condensation is important in order to determine the possible means by which to slow down or prevent the process from occurring. As a consequence, it is of great importance to understand the Hofmeister effect on the phase diagram and crystal nucleation rate of aqueous solutions of proteins. In this paper, we focus on the role of salt on equilibrium properties; in particular, we calculate the phase diagram of lysozyme for both sodium chloride and sodium thiocyanate, using a recent calculation of the lysozyme potential of mean force (PMF) that includes the effect of the ion-dispersion forces for these salts [17]. Their calculation of the PMF also includes a screened Coulomb interaction between the lysozyme molecules. In Ref. [17], Boström *et al.* have shown that the inclusion of ion-specific dispersion potentials gives rise to ion-specific phase diagrams, as one would expect for systems that exhibit the Hofmeister effect. Boström *et al.* examined a model for which they considered the effect of three distinct monovalent salts with different anions on the phase diagram of the solute: NaCl, NaSCN, and NaI. Their results show that the potentials of mean force between the lysozyme molecules become more attractive from NaCl to NaI to NaSCN, which is consistent with the experimental observation that NaSCN is more effective in precipitating hen-egg-white (HEW) lysozyme. Using their salt-based PMF contribution to the total potential, they calculated phase diagrams for the three electrolyte solutions by using a first-order Barker-Henderson perturbation theory [18,19] for the liquid and the solid phases, and they found that the three phase diagrams were qualitatively different. In particular, they found that the liquid-liquid curve was stable with respect to the solubility curve for NaCl and metastable for NaSCN.

It is well known that a first-order perturbation theory is not quantitatively accurate; thus it is of interest to obtain more accurate phase diagrams for these systems. In this paper, we address this question using the Boström *et al.* model [17] for two salts, NaCl and NaSCN, to predict the corresponding phase diagrams using systematic Monte Carlo techniques. In particular, we investigate the predicted stability and metastability of the fluid-fluid phase for NaCl and NaSCN, respectively, obtained from perturbation theory. Our results show that in contrast to the prediction of perturbation theory, the fluid-fluid phase separation curve is metastable

for the case of NaCl. In addition, the metastability gap we obtain for the case of NaSCN is greater than predicted by perturbation theory.

The remainder of the paper is as follows. In Sec. II we summarize the model, while in Sec. III we review the relevant simulation techniques necessary to obtain the liquid-liquid and liquid-solid phase diagrams. In Secs. IV and V, we present a discussion of our resulting phase diagrams and a brief conclusion, respectively.

II. MODEL AND SIMULATION TECHNIQUES

A. Model

Using Monte Carlo simulations, Boström *et al.* [17] calculated the PMF, W_{MC}, between two macroions that mimic lysozyme molecules in an aqueous salt solution, by fixing the distance between the macroions and allowing the small salt ions to move. The calculation included contributions from the ion-ion, ion-macroion, and macroion-macroion electrostatic interactions. In addition, they considered contributions from ion-ion and ion-macroion dispersion forces. The macroion-macroion van der Waals dispersion interaction was not included in the Monte Carlo calculation, but added separately. The concentration of the salts was held constant at 0.2 M. At this relatively large salt concentration, the Debye length is such that the electrostatic forces are strongly screened. Consequently, ion dispersion forces dominate the electrostatic forces in this regime. They repeated the simulation for different macroion separations and thus determined the PMFs for the three different salts. The solute particle was chosen to mimic properties of HEW lysozyme, i.e., it has a net charge of $10e$ and a diameter of 3.3 nm. The total interaction between two lysozyme molecules in the aqueous solution obtained in Ref. [17] is the sum of a hard-core interaction, W_{HS}, the potential of mean force obtained from a Monte Carlo simulation, W_{MC}, and the protein-protein van der Waals (Hamaker) dispersion interaction, W_{vdW}, i.e.,

$$W_{tot} = W_{HS} + W_{MC} + W_{vdW}, \tag{1}$$

where

$$W_{vdW}(r) = -\frac{H}{12}\left[\frac{\sigma^2}{r^2-\sigma^2} + \frac{\sigma^2}{r^2} + 2\ln\left(1-\frac{\sigma^2}{r^2}\right)\right], \quad r > \sigma + 2\kappa \tag{2}$$

and

$$W_{vdW}(r) = W_{vdW}(\sigma + 2\kappa), \quad \sigma < r \leqslant \sigma + 2\kappa. \tag{3}$$

The hard-sphere potential is infinite for $r<\sigma$ and zero otherwise. The potential W_{MC} is set to zero for $r>1.3\sigma$. The lysozyme-lysozyme dispersion interaction assumes a hydration-layer thickness of $\kappa=1.5$ Å and a Hamaker constant of $H=10kT_0$, where $T_0=298$ K. In addition, the total potential is assumed to be temperature independent for the range of temperatures that we study [17]. In Fig. 1, we have plotted the total potential, W_{tot}, for the NaCl and NaCSN electrolyte cases. The potential between the macroions becomes more attractive from NaCl to NaSCN, which is consistent with experimental observation that NaSCN is more effective in precipitating hen-egg white lysozyme than, for example, NaCl. We note that the model of Boström *et al.* has two discontinuities, as shown in Fig. 1. The first originates from the discontinuity intrinsic to W_{vdW} at $r=1.0909\sigma$. Bostrom *et al.* refer to Ref. [20], which argues that since the dispersion potential is based on a continuum approximation for the solvent that is invalid for surface-to-surface separations on the order of a solvent diameter, the hydration layer thickness κ determines the limit of validity of the van der Waals interaction. This is the reason for the cutoff used for W_{vdW}. The reason for introducing the second cutoff in W_{MC} at $r=1.3\sigma$ is simply that this potential is essentially zero beyond this point. We also note that it is possible that a different model, obtained by a different approximation for W_{vdW} at $r=1.0909\sigma$, could have an effect on the phase diagram, but this is beyond the scope of our current study.

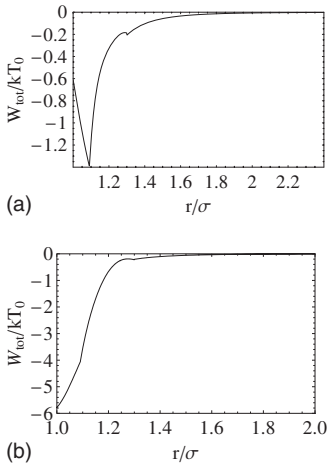

FIG. 1. Total lysozyme potentials for the (a) NaCl and (b) NaSCN electrolyte cases.

B. Simulation techniques

All of our Monte Carlo simulations for W_{tot} were conducted for a system of 512 particles in cubic boxes subject to periodic boundary conditions. The same number of Monte Carlo steps were performed for both equilibration and production, although the total number varied depending on the type of simulation. For all simulations, we set $\sigma=1$ and so the subsequent equations containing terms in ρ are to be interpreted as the reduced number density, i.e., $\tilde{\rho}=\rho\sigma^3$ with $\sigma=1$.

1. Fluid-fluid coexistence

We used the Gibbs ensemble Monte Carlo method [21,22] to obtain the fluid-fluid coexistence curve. This method avoids problems associated with the formation of an interface between the dense and dilute fluid phases. Two physically separate but thermodynamically connected simulation cells are used to mimic the two fluid phases. Standard particle displacements are performed within each simulation cell; in addition, volume and particle exchange are performed between the two cells. These exchanges are chosen

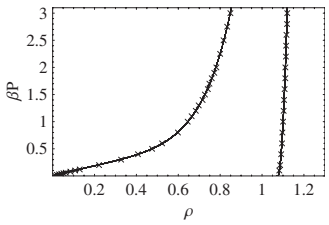

FIG. 2. Liquid and solid isotherms for NaCl at $T/T_0=1.0$. × are the Monte Carlo simulation results and the solid curves are the fits to the data.

such that the total volume and number of particles of the system are conserved and the simulations obey detailed balance. On average, we chose the ratio of particle displacements to volume moves to be 512:1; the frequency of particle transfers was chosen to give reasonable acceptance rates of approximately 1–5 %. The equilibrium and production run times were at least one billion Monte Carlo steps (MCS) each, with a MCS being an attempt at one of three possible moves: particle displacement, volume change, or particle exchange.

2. Fluid-solid coexistence

Fluid-solid coexistence curves can often be determined via the Gibbs-Duhem method [23]. This method involves integrating the first-order Clausius-Clapeyron equation

$$\frac{dP}{d\beta} = -\frac{\Delta h}{\beta \Delta v}, \tag{4}$$

where P is the pressure and $\beta=1/kT$. Δ indicates a difference between the two coexisting phases, i.e., liquid and solid phases in this case. Thus Δh and Δv are the differences in the molar enthalpies and molar volumes, respectively, of the two phases. One caveat to this approach is that it requires the knowledge of an initial coexistence point on the βP-$\beta\mu$ plane; see Fig. 4 for example. Consequently, we carried out a series of NPT simulations along an isotherm to determine the equation of state for both the fluid and solid phases. We show in Fig. 2 our results for the liquid and solid isotherms (for the NaCl solution) at a particular temperature. The equilibrium and production times for each NPT simulation were taken to be equal and at least 400 million MCS.

The isotherms were then fitted to the following forms:

$$\beta P = \frac{\rho}{(1-a\rho)} + b\left(\frac{\rho}{1-a\rho}\right)^2 + c\left(\frac{\rho}{1-a\rho}\right)^3 \quad \text{(liquid)}, \tag{5}$$

$$\beta P = a\rho^2 + b\rho + c \quad \text{(solid)}, \tag{6}$$

where ρ is the number density. Equations (5) and (6) are integrated to yield free energy for the corresponding state, and since

$$\beta\mu = \beta f + \beta\frac{P}{\rho}, \tag{7}$$

we can obtain the equations for the chemical potential,

TABLE I. Best-fit parameters for isotherms.

Salt	Isotherm	a	b	c
NaCl	Liquid	0.5482	−0.9596	0.9599
	Solid	1410.16	−3028.45	1625.95
NaSCN	Liquid	0.5008	−0.9942	0.8016
	Solid	1371.90	−3136.56	1789.48

$$\beta\mu_l = \ln\left(\frac{\rho\Lambda^2}{1-a\rho}\right) + \frac{b/a - c/a^2 + 1}{1-a\rho} + \frac{c/2a^2 + b\rho}{(1-a\rho)^2} + \frac{c\rho^2}{(1-a\rho)^3} - (b/a - c/2a^2 + 1), \tag{8}$$

$$\beta\mu_s = 2a\rho + b(\ln\rho + 1) - (a\rho^* + b\ln\rho^* - c/\rho^*) + \beta f^{\text{ex}}(\rho^*) + \ln(\Lambda^2\rho^*) - 1, \tag{9}$$

where $\Lambda=\sqrt{h^2/2\pi kT}$ is the thermal de Broglie wavelength. The value of Λ plays no role in the location of phase equilibria for classical systems. Table I shows the parameters that best fit our Monte Carlo data for the liquid and solid isotherms for the two salts.

The ρ^* in Eq. (9) is a result of the integration and denotes a reference state whose free energy must be predetermined from a series of independent simulations. To calculate this, we use the Frenkel-Ladd method [24] to harmonically couple lysozyme particles to a lattice, i.e., an Einstein crystal. The potential energy of this system is

$$W(\lambda) = W_{\text{tot}} + \lambda\sum_{i=1}^{N}(\vec{r}_i - \vec{r}_{0,i})^2, \tag{10}$$

where $\vec{r}_{0,i}$ is the position of the lattice site to which particle i is coupled, $\vec{r}_i$ is the position of the particle, and λ is the coupling parameter. The free energy of the lysozyme system is then

$$F_{\text{Lys}} = F_{\lambda_{\max}} - \int_0^{\lambda_{\max}} d\lambda\langle W(r,\lambda)\rangle_\lambda = F_{\lambda_{\max}} - \int_0^{\lambda_{\max}} d\lambda\left\langle\sum_{i=1}^{N}(\vec{r}_i - \vec{r}_{0,i})^2\right\rangle_\lambda. \tag{11}$$

At sufficiently high values of $\lambda_{\max}$, i.e., the coupling is sufficiently strong, the system behaves as a noninteracting Einstein crystal, the free energy of which can be calculated exactly. We can then obtain F_{Lys} via thermodynamic integration along a reversible path. The mean-squared displacement of particles relative to their lattice positions is calculated by simulation in a system with a fixed center of mass. In Fig. 3, we show the relative mean-squared displacement as a function of the coupling parameter. It can be seen that for sufficiently large λ, the system behaves as an Einstein lattice and thus the reversible path has been established.

Once the chemical potentials of both phases are obtained at the same temperature, we obtain the coexistence points by equating the chemical potential and the pressure for the two phases (Fig. 4). We denote the coexisting temperature and

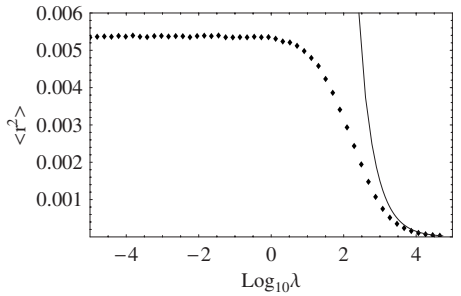

FIG. 3. Monte Carlo data of the mean-squared displacements for the coupled solid in the NaCl system (diamonds) compared with that of an Einstein lattice (solid line). To achieve deviations of less than 1% with the Einstein lattice, a λ_{max} of 260 000 was required.

pressure to be T_1 and P_1, respectively. We then use the Gibbs-Duhem method to generate the entire coexistence curve. A simple predictor-corrector algorithm was used for the integration. The basic idea is as follows. Since h and v at (T_1, P_1) can be obtained conveniently from our previous simulations for the coexisting densities, equation (11) can then be used to estimate the coexisting pressure $P_{2,\mathrm{est}}$ for the next temperature T_2 (prediction). Next, two *NPT* simulations are executed in parallel at $(T_2, P_{2,\mathrm{est}})$ and we obtain another set of h and v values. By taking the average of the two sets of h's and v's, we obtain a more accurate estimate for P_2 (correction). Finally, two new *NPT* simulations at (T_2, P_2) are carried out to give the coexisting densities at T_2. This process is repeated until the entire fluid-solid coexistence curve is obtained.

III. RESULTS

Our Monte Carlo results yield a metastable fluid-fluid phase for the 0.2 M NaCl lysozyme solution, Fig. 5. This is not surprising since the range of attraction is small with respect to the particle diameter. It is known in the case of square-well fluids that the threshold for metastability begins for ranges less than about 1.25σ [25]. Though the potentials we study are quite different from square wells, one can make a comparison following a treatment by Noro and Frenkel [26], in which the effective range of a potential is estimated by equating the reduced second virial coefficients, B_2^*, of a square-well system with the system in question. This yields an effective square-well range of approximately 1.13σ, so that our Monte Carlo prediction of a metastable fluid-fluid curve is consistent with the estimate of Noro and Frenkel. (In general, this effective range is temperature-dependent; however, the variation of B_2^* in the region of interest is small.) Another measure of the metastability of the phase separation curve is the so-called metastability gap, defined as $(T_L - T_c)/T_c$. For NaCl, we find that this gap is 8.1%.

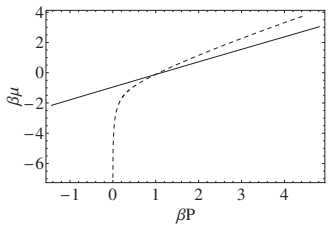

FIG. 4. $\beta P - \beta\mu$ plot for the NaSCN system at $\frac{T}{T_0} = 3.5$. Dashed line for liquid; solid line for solid.

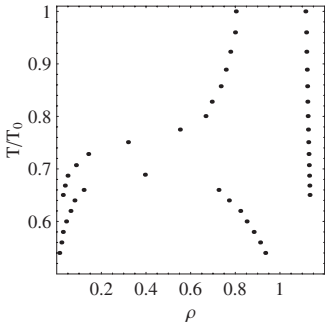

FIG. 5. Phase diagram obtained from Monte Carlo simulations for the aqueous lysozyme solution with NaCl electrolyte at 0.2 M. The fluid-fluid separation curve is metastable.

The phase diagram for the 0.2 M NaSCN lysozyme solution is shown in Fig. 6. Again, following the treatment of Noro and Frenkel, we estimate the effective range to be approximately 1.13σ. The metastability gap for NaSCN is estimated to be 18%, which is much bigger than the 5% estimated from perturbation theory. In both the NaCl and NaSCN cases, the effective range falls within the region of metastability for square-well fluids [25].

Estimates of the critical points for our finite system were obtained by fitting the fluid-fluid coexistence data to the following equations:

$$\frac{\rho_l + \rho_g}{2} \simeq \rho_c + A|T - T_c|, \tag{12}$$

$$\rho_l - \rho_g \simeq B|T - T_c|^{\beta}, \tag{13}$$

where T_c and ρ_c are the critical temperature and density, respectively, and $\beta \simeq 0.326$ is the 3D-Ising critical exponent. Finite-size effects would have to be taken into account to obtain the critical point parameters for the infinite system. Table II contains a summary of the critical parameters and fitting parameters for the two systems investigated.

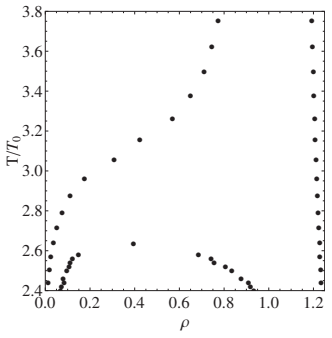

FIG. 6. Phase diagram curve obtained from Monte Carlo simulations for the aqueous lysozyme solution with NaSCN electrolyte at 0.2 M. The fluid-fluid separation curve is metastable.

TABLE II. Critical parameters.

Salt	T_c/T_0	ρ_c	A	B	B_2^*
NaCl	0.700	0.392	0.54	1.69	−1.42
NaSCN	2.636	0.395	0.48	1.40	−1.40

In addition, we have calculated the reduced second virial coefficients at their respective critical temperatures,

$$B_2{}^* \equiv B_2/B_{2\mathrm{HS}} = 1 + 3\int_1^\infty s^2(1 - e^{-\beta W_{\mathrm{tot}}(s)})ds, \qquad (14)$$

where $s \equiv r/\sigma$ for each system. In both salt cases, B_2^* is small and negative, consistent with experimental observations for systems that undergo metastable fluid-fluid transitions. In particular, for lysozyme solutions with 0.2 M NaCl, the experimental reduced second virial coefficient is estimated to be −0.5 (see, e.g., Ref. [32]).

To the best of our knowledge, no experimental data exist for a 0.2 M NaCl lysozyme solution, nor do any experimental data on phase diagrams exist for NaSCN lysozyme solutions. However, for solutions with 0.5 M or greater concentrations of NaCl, experimental data are available. This data do indeed show the presence of a metastable fluid-fluid phase for salt concentrations greater than 0.5 M [27].

IV. CONCLUSION

Our predicted phase diagrams for NaCl and NaSCN lysozyme solutions have been obtained using standard Monte Carlo techniques. It is clear that the model we study is an improvement over earlier models of lysozyme in that it can account at least qualitatively for the Hofmeister effect. However, we find that our results are rather different from those predicted by Boström *et al.*, as one might expect. In both the NaCl and NaSCN cases, the liquid-liquid curve is metastable with respect to the liquid-solid transition. In contrast to their predictions using first-order perturbation theory, our Monte Carlo results show that the liquid-liquid curve for the NaCl system is metastable with a gap of 8%. In the case of NaSCN, our results show a larger metastability gap than obtained from the perturbation theory; the Monte Carlo results yield a gap of 18%. It should also be noted that although the effective range (as defined in Sec. III and Ref. [26]) and reduced second virial coefficient are almost the same for the NaCl and NaSCN models, details such as T_c/T_0 and the metastability gap are rather different. This is due to the quantitative differences between the potentials of mean force for the two models, such as the much larger well depth for the NaSCN case.

It is possible that the potential of mean force calculated in Ref. [17] needs to be improved. For example, the model for the protein could be improved to take into account a more realistic description of the amino acid charge distribution on the protein surface. Another effect that might need to be investigated is the effect of the buffer on the potential of mean force. The buffer is usually added to obtain the right pH, otherwise it is assumed to have no further influence, but it is conceivable that there could be large buffer effects on the potential of mean force [28]. Further, it is possible that isotropic models such as these (i.e., models that are independent of macromolecule orientation) cannot account for such quantitative features as the breadth of the coexistence curve, and that one must take into account the effects of anisotropy [29–31] on the interactions that can arise from a variety of sources, including that of water.

ACKNOWLEDGMENTS

This work is supported by grants from the Harold G. and Leila Y. Mathers Charitable Foundation and the National Science Foundation (Grant No. DMR-0702890).

[1] F. Hofmeister, Arch. Exp. Pathol. Pharmacol. **24**, 247 (1888).
[2] J. D. Gunton, A. Shiryayev, and D. L. Pagan, *Protein Condensation: Kinetic Pathways to Crystallization and Disease* (Cambridge University Press, Cambridge, 2007),
[3] M. Boström, D. R. M. Williams, and B. W. Ninham, Phys. Rev. Lett. **87**, 168103 (2001).
[4] B. W. Ninham and V. Yaminsky, Langmuir **13**, 2097 (1997).
[5] M. Boström, B. W. Ninham, and D. Williams, Biophys. J. **85**, 686 (2003).
[6] Y. Zhang and P. S. Cremer, Curr. Opin. Chem. Biol. **10**, 658 (2006).
[7] W. Kunz, P. Lo Nostro, and B. W. Ninham, Curr. Opin. Colloid Interface Sci. **9**, 1 (2004).
[8] F. W. Tavares *et al.*, J. Phys. Chem. B **108**, 9228 (2004).
[9] M. Boström *et al.*, J. Phys. Chem. B **109**, 24489 (2005).
[10] M. S. Turner, R. W. Briehl, F. A. Ferrone, and R. Josephs, Phys. Rev. Lett. **90**, 128103 (2003).
[11] C. W. Jones, J. C. Wang, F. A. Ferrone, R. W. Briehl, and M. S. Turner, Faraday Discuss. **123**, 221 (2003).
[12] R. Mirchev and F. A. Ferrone, J. Mol. Biol. **265**, 475 (1997).
[13] G. B. Benedek, Invest. Ophthalmol. Visual Sci. **38**, 1911 (1997).
[14] A. Stradner, G. Foffi, N. Dorsaz, G. Thurston, and P. Schurtenberger, Phys. Rev. Lett. **99**, 198103 (2007).
[15] Y. M. Kuo *et al.*, J. Biol. Chem. **271**, 4077 (1996).
[16] S. A. Gravina *et al.*, J. Biol. Chem. **270**, 7013 (1995).
[17] M. Boström, F. Tavares, B. Ninham, and J. Prausnitz, J. Phys. Chem. B **110**, 24757 (2006).
[18] J. A. Barker and D. Henderson, J. Chem. Phys. **47**, 4714 (1967).
[19] D. Henderson and J. A. Barker, Phys. Rev. A **1**, 1266 (1970).
[20] R. A. Curtis, J. Ulrich, A. Montaser, J. M. Prausnitz, and H. W. Blanch, Biotechnol. Bioeng. **79**, 367 (2002).
[21] D. Frenkel and B. Smit, *Understanding Molecular Simulation: From Algorithms to Applications* (Academic, Boston, 1996).
[22] A. Z. Panagiotopoulos, Mol. Phys. **61**, 813 (1987).

[23] D. A. Kofke, J. Chem. Phys. **98**, 4149 (1993); Mol. Phys. **78**, 1331 (1993).
[24] D. Frenkel and A. J. C. Ladd, J. Chem. Phys. **81**, 3188 (1984).
[25] D. L. Pagan and J. D. Gunton, J. Chem. Phys. **122**, 184515 (2005).
[26] M. G. Noro and D. Frenkel, J. Chem. Phys. **113**, 2941 (2000).
[27] M. Muschol and F. Rosenberger, J. Chem. Phys. **107**, 1953 (1997).
[28] A. Striolo *et al.*, Phys. Chem. Chem. Phys. **5**, 4851 (2003).
[29] N. Kern and D. Frenkel, J. Chem. Phys. **118**, 9882 (2003).
[30] X. Song, Phys. Rev. E **66**, 011909 (2002).
[31] Riccardo Fantoni *et al.*, J. Chem. Phys. **127**, 234507 (2007).
[32] P. Prinsen and T. Odijk, J. Chem. Phys. **121**, 6525 (2004).